

**Supplementary Information for**  
**Assessing the Roles of Synthesis Method and Chemical Composition in Determining**  
**Structure-Property Correlations in Alloyed, Ultrathin Nanowire Motifs for the Methanol**  
**Oxidation Reaction**

Scott C. McGuire,<sup>1,#</sup> Nathaniel R. Hurley,<sup>1,#</sup> Michael G. Gallagher,<sup>1</sup> Lihua Zhang,<sup>3</sup>

Anatoly I. Frenkel,<sup>2,4,\*</sup> and Stanislaus S. Wong<sup>1,\*</sup>

<sup>1</sup>Department of Chemistry, Stony Brook University,

Stony Brook, New York 11794-3400, USA

<sup>2</sup>Department of Materials Science and Chemical Engineering,

Stony Brook University, Stony Brook, New York 11794-2275, USA

<sup>3</sup>Center for Functional Nanomaterials,

Brookhaven National Laboratory, Upton, New York 11973, USA

<sup>4</sup>Chemistry Division, Brookhaven National Laboratory, Upton, New York 11973, USA

<sup>#</sup>These authors contributed equally to this manuscript.

<sup>\*</sup>To whom correspondence should be addressed.

Email: [anatoly.frenkel@stonybrook.edu](mailto:anatoly.frenkel@stonybrook.edu); [stanislaus.wong@stonybrook.edu](mailto:stanislaus.wong@stonybrook.edu)

## **Fuel Cell Background**

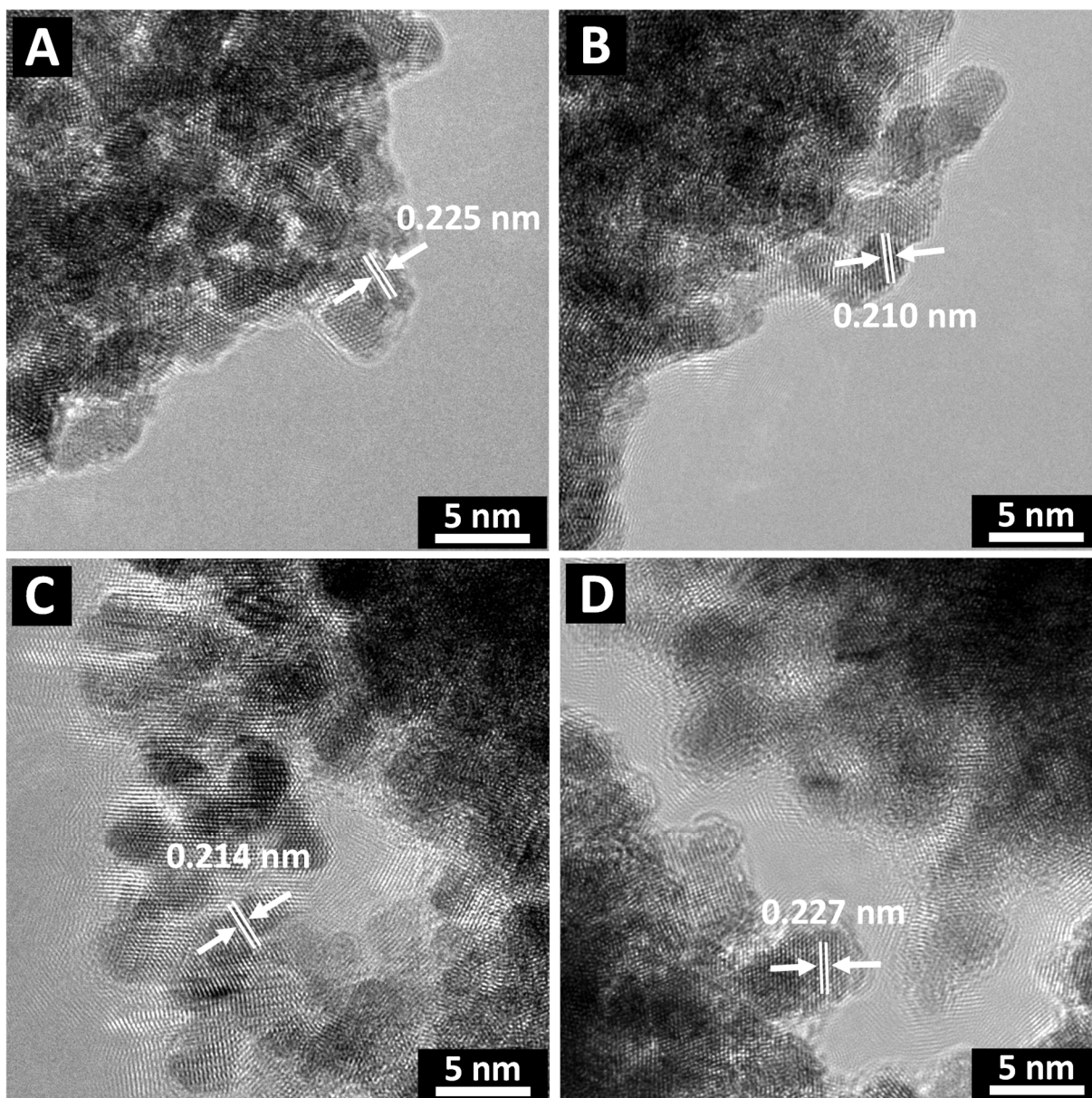
Fuel cell (FC) configurations convert chemical energy via an oxidation process (at the anode) with a corresponding reduction (at the cathode) of that fuel source, into electrical energy. In particular, direct alcohol fuel cell (DAFC) technology represents a potential fuel cell option for future applications in the automotive,<sup>1</sup> portable power,<sup>2,3</sup> and electronics industries.<sup>4,5</sup> However, in spite of this tremendous promise, today's DAFCs, including more specifically direct methanol fuel cells (DMFCs) and direct ethanol fuel cells (DEFCs), powered by methanol and ethanol, respectively, suffer from high production costs and relatively low efficiencies.<sup>6</sup> These shortfalls can be traced in large part to the metal-based catalysts that are employed at both the anode<sup>7-9</sup> and the cathode.<sup>10,11</sup>

## **Additional Comments on the SRO Parameter**

First, the total coordination numbers of the two atom types must be compared. In the case where  $N_A$  and  $N_B$  are equivalent, then there is no significant surface segregation of either atom type. On the other hand, if the total coordination for atoms A and B are not equivalent, then the atom type with the larger coordination number is likely to be more localized within the core, while the atom type with the lower coordination number is localized towards the surface. The SRO parameter can only be meaningfully compared in the case where the two total coordination numbers are equivalent and there is no noticeable surface segregation. The possible values for the SRO parameter are between -1 and 1. In the event where the SRO parameter is equal to -1, the local atomic structure is completely ordered. When the value is equal to 0, the material exists as a random, homogeneous alloy, where A atoms are just as likely to be next to B atoms as A

atoms. Finally, when the SRO parameter is equivalent to 1, there is no alloying, and it is suggestive of the formation of completely segregated A and B particles.

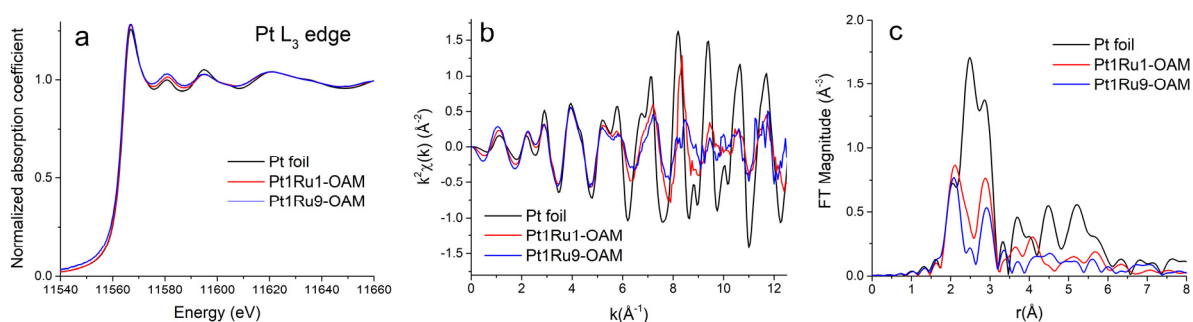
As a key precursor to this current paper, we have previously investigated<sup>12</sup> the local atomic structure of our as-prepared Ru<sub>2</sub>Co<sub>1</sub> NWs, in conjunction with analogous ultrathin Ru<sub>1</sub>Pt<sub>1</sub>, Au<sub>1</sub>Ag<sub>1</sub>, Pd<sub>1</sub>Pt<sub>1</sub>, and Pd<sub>1</sub>Pt<sub>9</sub> NWs which were generated as ‘controls’. Hence, analysis of EXAFS spectra yielded insights into the local coordination environment and provided an average picture of the entire sample. Specifically, we calculated structure-dependent Cowley-Warren short range order (SRO) ( $\alpha$ ) parameters as a means of characterizing the local distribution of elements throughout the alloyed nanowires. In a homogeneous alloy, when the SRO value is 0, the bimetallic components are randomly mixed at the atomic scale, whereas if the SRO is positive, there is a better tendency for the material to form segregated constituent components. We collected and ultimately weaved together a narrative comprising quantitative EDS, EDS mapping (with associated line scans), and EXAFS data, that reconciled the localized EDS information with the ensemble averaged picture provided by EXAFS of the distribution of atoms within a bimetallic system.



**SI Figure 1.** HRTEM images and lattice spacings of (A) Pt<sub>3</sub>Ru<sub>1</sub> CTAB, (B) Pt<sub>1</sub>Ru<sub>1</sub> CTAB, (C) Pt<sub>1</sub>Ru<sub>9</sub> OAm, and (D) Pt<sub>1</sub>Ru<sub>1</sub> OAm.

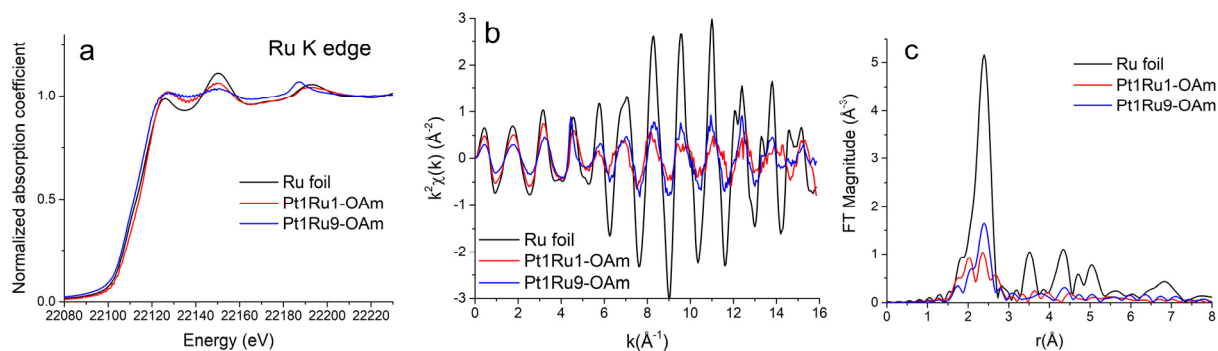
**Raw XANES and EXAFS data for Pt<sub>1</sub>Ru<sub>1</sub> - OAm / OA and Pt<sub>1</sub>Ru<sub>9</sub> - OAm / OA**

Pt L<sub>3</sub> edge XANES data for Pt<sub>1</sub>Ru<sub>1</sub> and Pt<sub>1</sub>Ru<sub>9</sub> mediated using the OAm / OA surfactant process are shown in SI Figure 1A. The k<sup>2</sup>-weighted EXAFS data in k-space and r-space (note: the Fourier transforms were done for the k<sup>2</sup>-weighted EXAFS spectra in the k-range from 2 to 12 Å<sup>-1</sup> using the Hanning window function and dk = 2 Å<sup>-1</sup>) are shown in Figures 1B and 1C, respectively.



**SI Figure 2.** (a) Pt L<sub>3</sub>-edge XANES data, (b) k<sup>2</sup>-weighted EXAFS data in k-space, and (c) Fourier transform magnitudes of the k<sup>2</sup>-weighted EXAFS data for the Pt foil in addition to both Pt<sub>1</sub>Ru<sub>1</sub> and Pt<sub>1</sub>Ru<sub>9</sub>, prepared by the OAm/OA synthesis process.

Ru K-edge XANES data for Pt<sub>1</sub>Ru<sub>1</sub> and Pt<sub>1</sub>Ru<sub>9</sub> prepared using the OAm/OA surfactant are shown in SI Figure 2A. The  $k^2$ -weighted EXAFS data in  $k$ -space and  $r$ -space (the Fourier transforms were performed for the  $k^2$ -weighted EXAFS spectra in the  $k$ -range from 2 to 15  $\text{\AA}^{-1}$  using Hanning window function and  $dk = 2 \text{\AA}^{-1}$ ) are shown in Figures 2B and C, respectively.



**SI Figure 3.** (a) Ru K-edge XANES data, (b)  $k^2$ -weighted EXAFS data in  $k$ -space, and (c) Fourier transform magnitudes of the  $k^2$ -weighted EXAFS data for the Ru foil in addition to both Pt<sub>1</sub>Ru<sub>1</sub> and Pt<sub>1</sub>Ru<sub>9</sub>, prepared by the OAm/OA synthesis process.

### Fit results for Pt foil, Ru foil and alloy samples

SI Table 1 presents the Hanning window ranges for Fourier transforms used in the fits and the fitting range in r-space. Given also are the r-factor of the fit and the constraints used in the multiple-edge data set fittings. SI Table 2 summarizes the fit results.

**SI Table 1.** Fitting parameters.

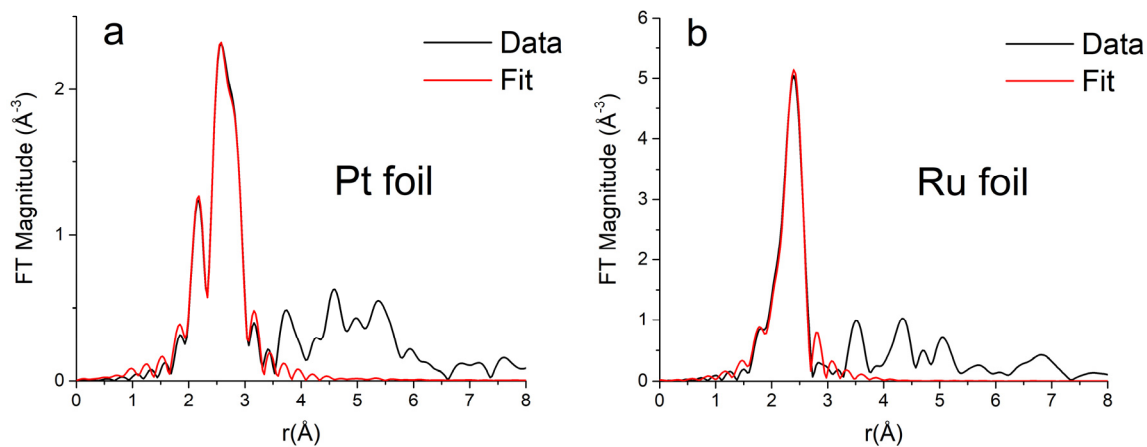
		k-range ( $\text{\AA}^{-1}$ )	r-range ( $\text{\AA}$ )	r-factor	Constraints
Pt foil	Pt L <sub>3</sub> edge	2.5-15	1.85-3.315	0.002	
Ru foil	Ru K edge	2-14.5	1.85-2.703	0.004	
Pt <sub>1</sub> Ru <sub>1</sub> - CTAB	Pt L <sub>3</sub> edge	2.5-14.5	1.85-3.315	0.026	$R_{\text{Pt-Ru}} = R_{\text{Ru-Pt}}$
	Ru K edge	2-14.5	1.85-2.915		$\sigma_{\text{Pt-Ru}}^2 = \sigma_{\text{Ru-Pt}}^2$
Pt <sub>3</sub> Ru <sub>1</sub> - CTAB	Pt L <sub>3</sub> edge	2.5-15	1.85-3.326	0.016	$R_{\text{Pt-Ru}} = R_{\text{Ru-Pt}}$
	Ru K edge	2-15	1.85-2.904		$\sigma_{\text{Pt-Ru}}^2 = \sigma_{\text{Ru-Pt}}^2$
Pt <sub>1</sub> Ru <sub>1</sub> -OAm	Pt L <sub>3</sub> edge	2.5-15.5	1.85-3.337	0.034	$R_{\text{Pt-Ru}} = R_{\text{Ru-Pt}}$
	Ru K edge	2-14.5	1.85-2.926		$\sigma_{\text{Pt-Ru}}^2 = \sigma_{\text{Ru-Pt}}^2$
Pt <sub>1</sub> Ru <sub>9</sub> -OAm	Pt L <sub>3</sub> edge	2.5-13.5	1.85-3.148	0.008	$R_{\text{Pt-Ru}} = R_{\text{Ru-Pt}}$
	Ru K edge	2-14.5	1.85-2.926		$\sigma_{\text{Pt-Ru}}^2 = \sigma_{\text{Ru-Pt}}^2$

**SI Table 2.** Fit results for the bimetallic alloys and reference Pt and Ru foils.

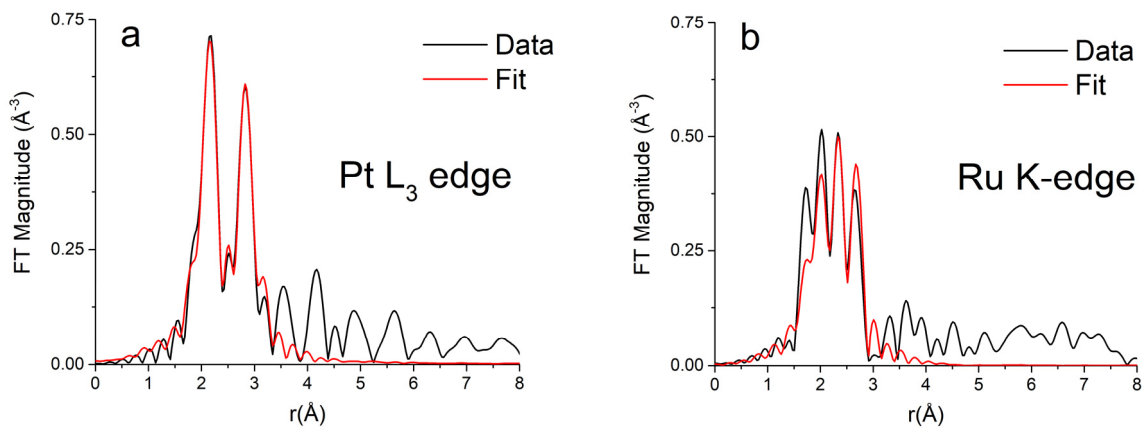
	Pt foil	Ru foil	Pt <sub>1</sub> Ru <sub>1</sub> - CTAB	Pt <sub>3</sub> Ru <sub>1</sub> - CTAB	Pt <sub>1</sub> Ru <sub>1</sub> - OAm	Pt <sub>1</sub> Ru <sub>9</sub> - OAm
$N_{\text{Pt-Pt}}$	12(f)		5.6(6)	5.6(3)	7.1(1.3)	7.7(1.8)
$N_{\text{Pt-Ru}}$			1.3(3)	0.8(2)	2.3(7)	2.0(9)
$N_{\text{Ru-Ru}}$		12(f)	2.4(6)	1.5(7)	5.4(1.1)	3.9(4)
$N_{\text{Ru-Pt}}$			1.9(5)	5.6(1.4)	2.7(9)	0.7(4)
$R_{\text{Pt-Pt}} (\text{\AA})$	2.765(1)		2.732(6)	2.737(3)	2.753(6)	2.74(1)
$R_{\text{Pt-Ru}} (\text{\AA})$			2.708(8)	2.702(8)	2.72(1)	2.69(2)
$R_{\text{Ru-Ru}} (\text{\AA})$		2.677(3)	2.676(8)	2.64(1)	2.688(9)	2.672(4)
$\sigma_{\text{Pt-Pt}}^2 (\text{\AA}^2)$	0.0049(1)		0.0065(7)	0.0071(3)	0.004(1)	0.008(2)
$\sigma_{\text{Pt-Ru}}^2 (\text{\AA}^2)$			0.004(1)	0.007(1)	0.004(1)	0.005(2)
$\sigma_{\text{Ru-Ru}}^2 (\text{\AA}^2)$		0.0039(4)	0.006(1)	0.003(2)	0.007(1)	0.0038(6)



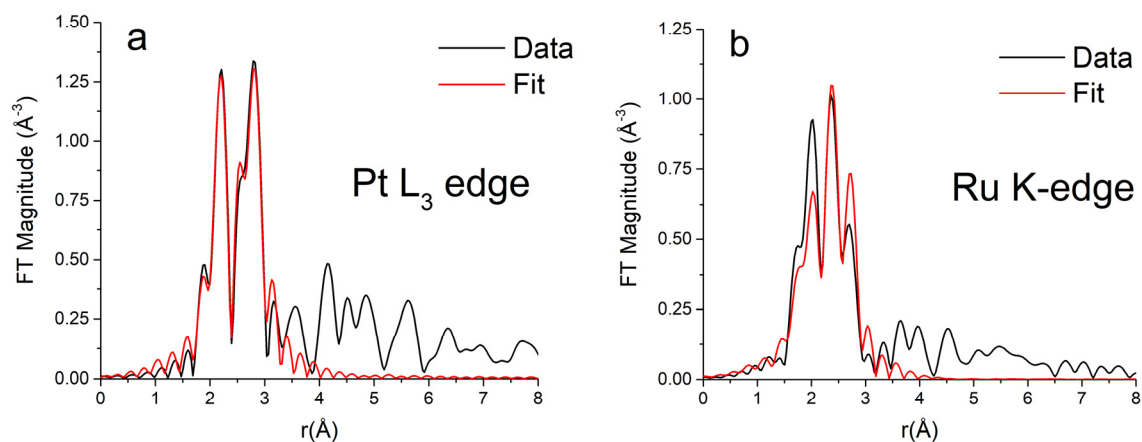
The data and the fits for the reference Pt and Ru foils in addition to Pt<sub>1</sub>Ru<sub>1</sub> prepared using the CTAB process as well as Pt<sub>1</sub>Ru<sub>1</sub> and Pt<sub>1</sub>Ru<sub>9</sub> samples, generated using OAm/OA surfactants, are shown in SI Figures 3 (A, B), 4, 5, and 6, respectively.



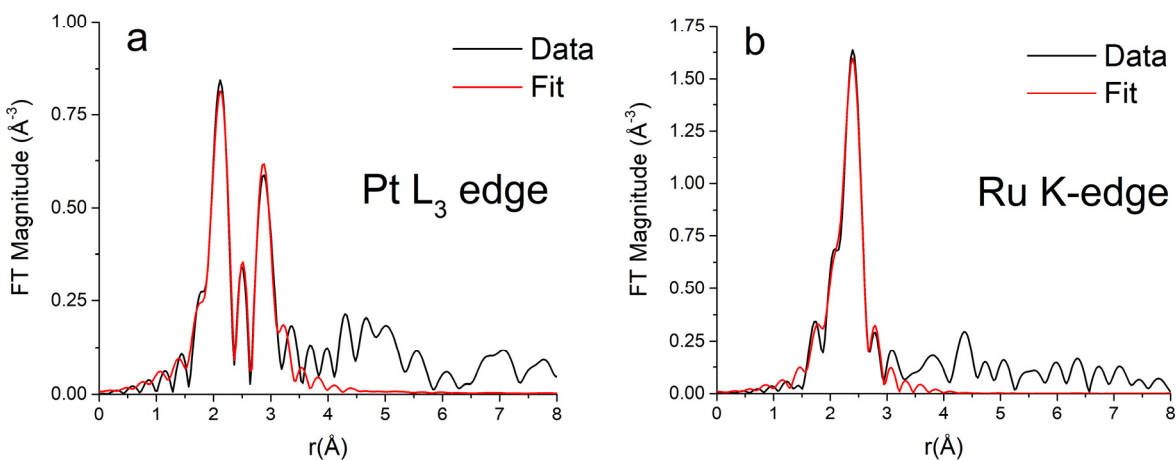
**SI Figure 4.** Fourier transform magnitudes of  $k^2$ -weighted EXAFS data and theoretical fits for (A) Pt foil at the L<sub>3</sub>-edge and (B) Ru foil at the K-edge.



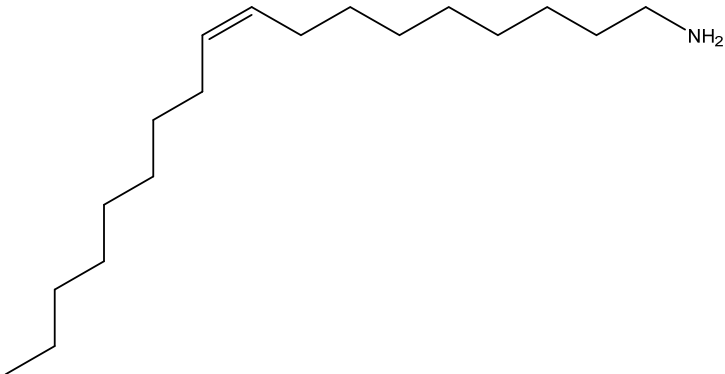
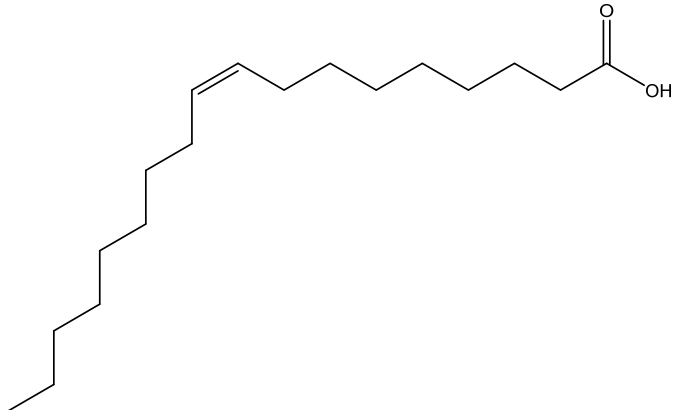
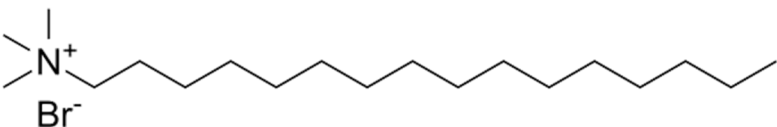
**SI Figure 5.** Fourier transform magnitudes of  $k^2$ -weighted EXAFS data and theoretical fits for the Pt<sub>1</sub>Ru<sub>1</sub> (prepared using CTAB) sample at the (A) Pt L<sub>3</sub>-edge and (B) Ru K-edge.



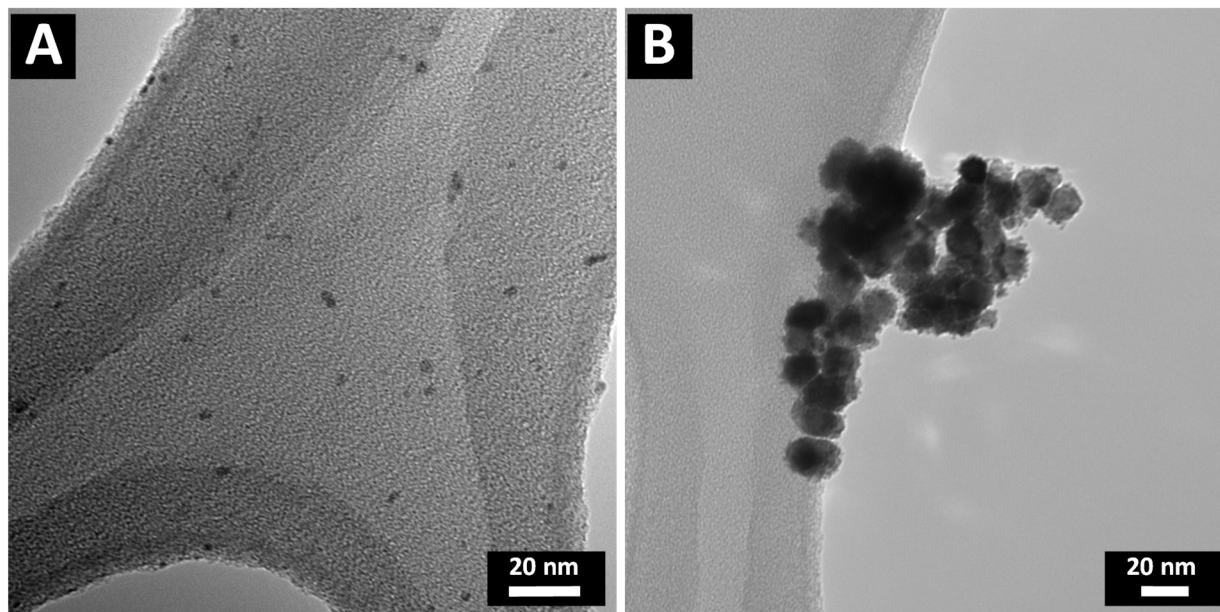
**SI Figure 6.** Fourier transform magnitudes of  $k^2$ -weighted EXAFS data and theoretical fits for the Pt<sub>1</sub>Ru<sub>1</sub> (prepared with OAm/OA) sample at (A) the Pt L<sub>3</sub>-edge and (B) the Ru K-edge.



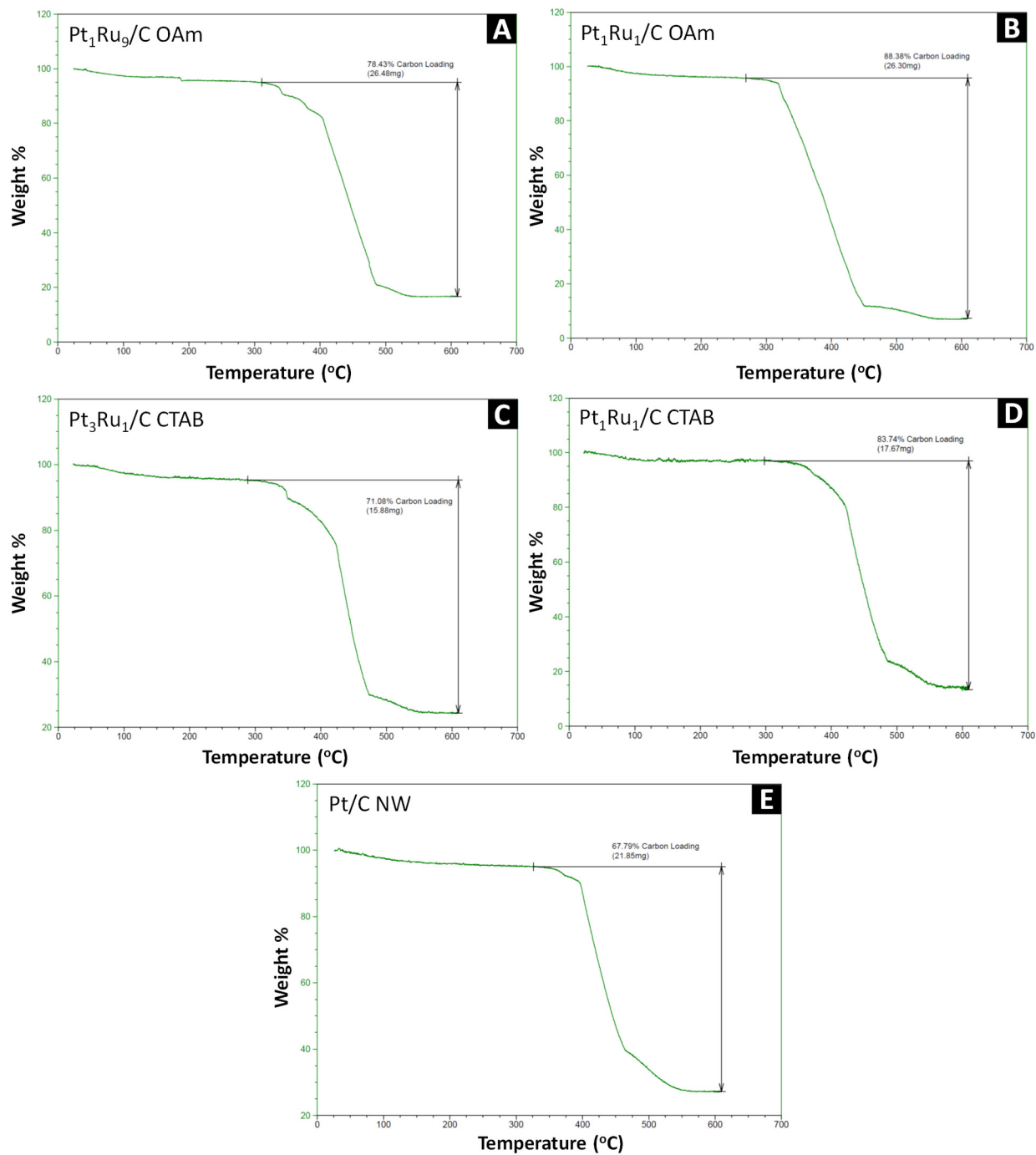
**SI Figure 7.** Fourier transform magnitudes of  $k^2$ -weighted EXAFS data and theoretical fits for the Pt<sub>1</sub>Ru<sub>9</sub> (prepared with OAm/OA) sample at (A) the Pt L<sub>3</sub>-edge and (B) the Ru K-edge.

Surfactant	Structure
Oleylamine (OAm)	
Oleic Acid (OAc)	
Hexadecyltrimethylammonium Bromide (CTAB)	

**SI Table 3.** Surfactants, abbreviations, and associated chemical structures (made in Chemdraw).



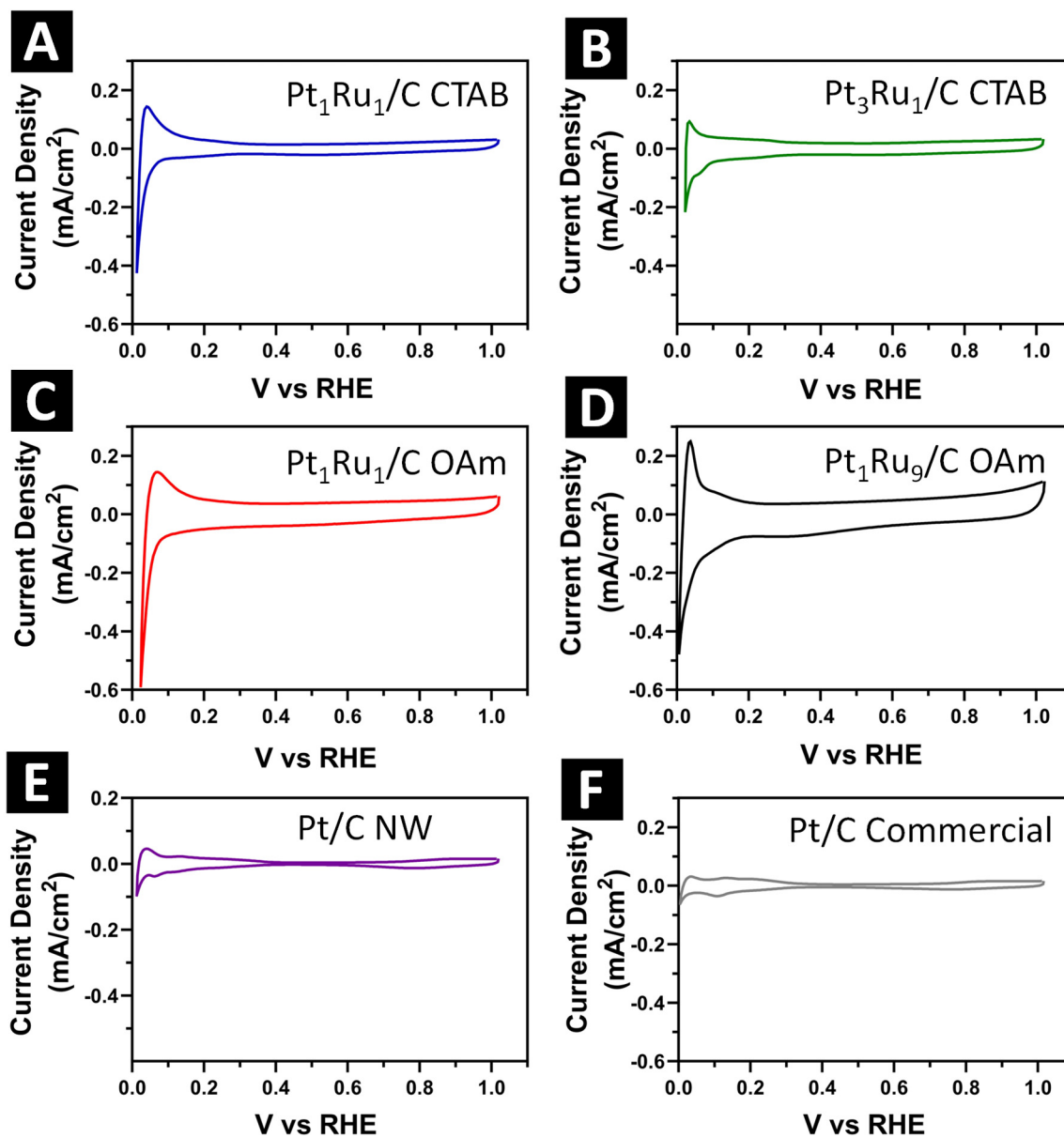
**SI Figure 8.** TEM images of (A)  $\text{Pt}_1\text{Ru}_9$  created by the CTAB method and (B)  $\text{Pt}_3\text{Ru}_1$  created by the OAm /OA process.



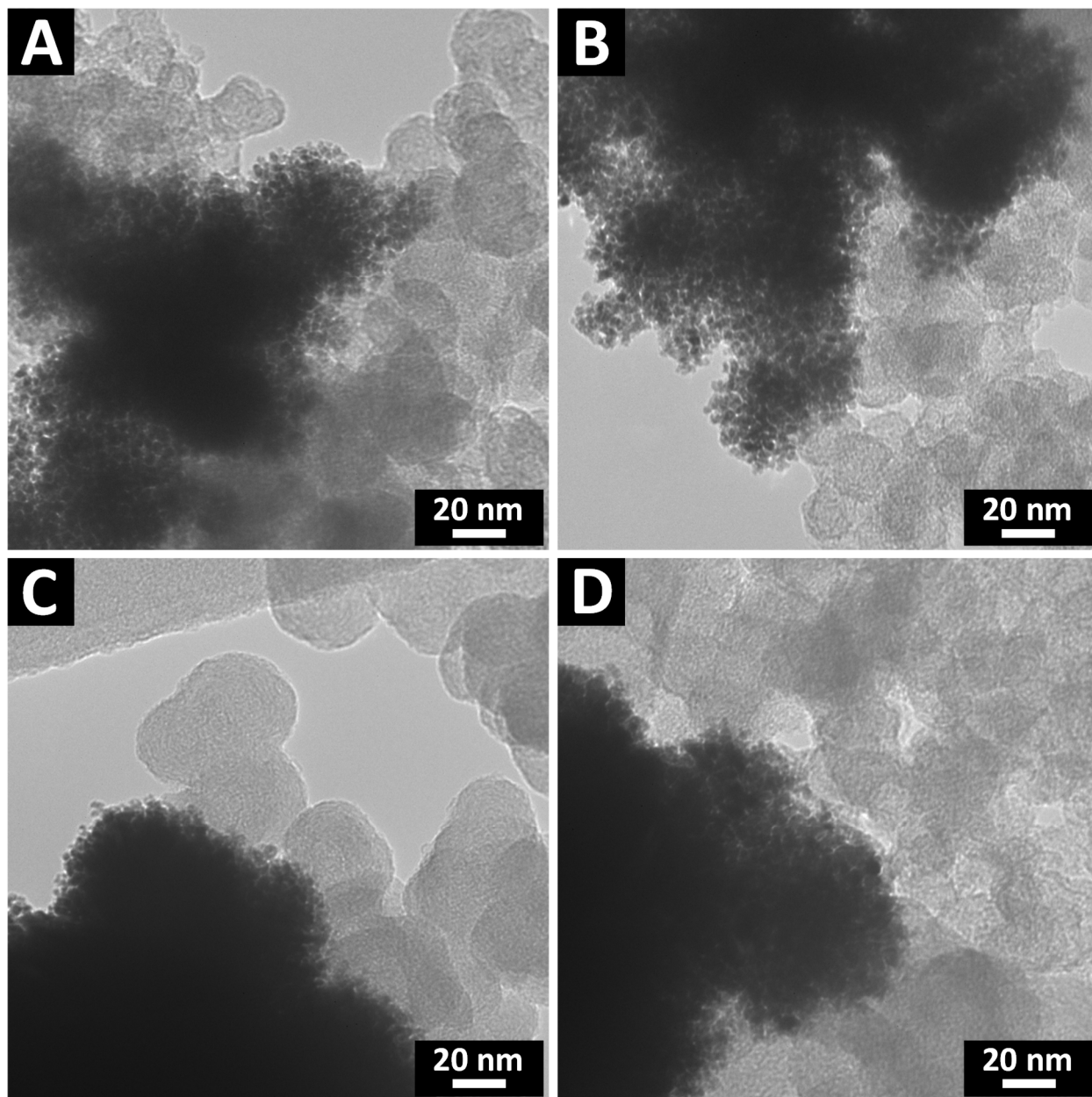
**SI Figure 9.** TGA data of various as-synthesized samples loaded onto Vulcan carbon in separate runs, including (A) Pt<sub>1</sub>Ru<sub>9</sub> OAm, (B) Pt<sub>1</sub>Ru<sub>1</sub> OAm, (C) Pt<sub>1</sub>Ru<sub>1</sub> CTAB, (D) Pt<sub>1</sub>Ru<sub>1</sub> CTAB, and (E) Pt/C NW respectively.

Sample	SA (mA/cm <sup>2</sup> )	SSA (m <sup>2</sup> /g)
Pt <sub>3</sub> Ru <sub>1</sub> CTAB	1.22	4.74
Pt <sub>1</sub> Ru <sub>1</sub> CTAB	0.55	7.82
Pt <sub>1</sub> Ru <sub>1</sub> OAm	0.46	4.77
Pt <sub>1</sub> Ru <sub>9</sub> OAm	0.07	5.31
Pt pure CTAB	0.17	20.81
Pt/C commercial standard	0.17	74.21

**SI Table 4.** Average specific activities and specific surface areas of as-synthesized nanowires and particles. SA values were taken at 0.7 V vs RHE. Both SA and SSA were averaged over 3 measurements.

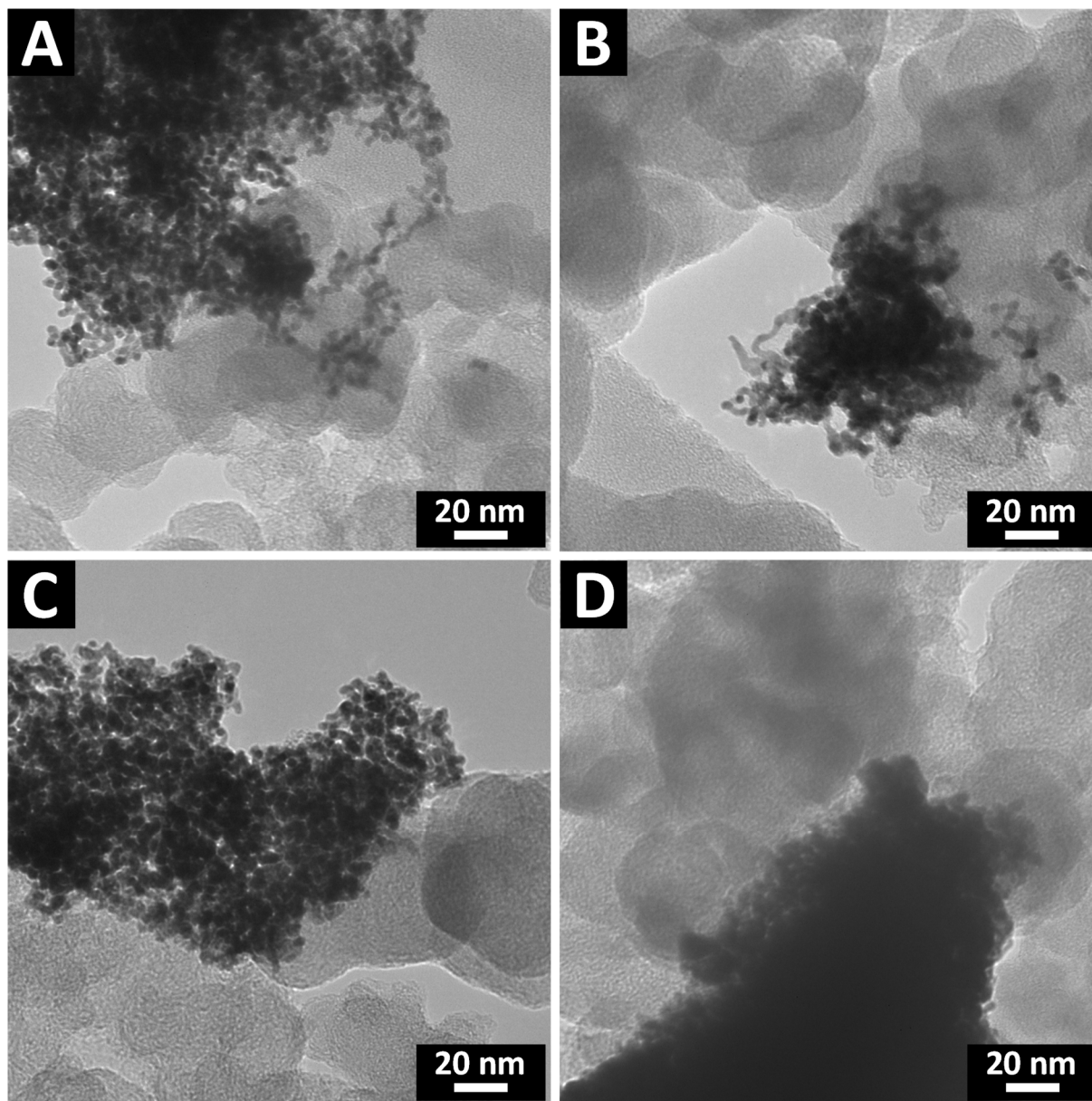


**SI Figure 10.** CV curves of samples of as-prepared PtRu alloys, deposited onto carbon, including (A) Pt<sub>1</sub>Ru<sub>1</sub>/C CTAB, (B) Pt<sub>3</sub>Ru<sub>1</sub>/C CTAB, (C) Pt<sub>1</sub>Ru<sub>1</sub>/C OAm, (D) Pt<sub>1</sub>Ru<sub>9</sub>/C OAm, (E) pure Pt/C NWs, and (F) Pt/C commercial standard, respectively.

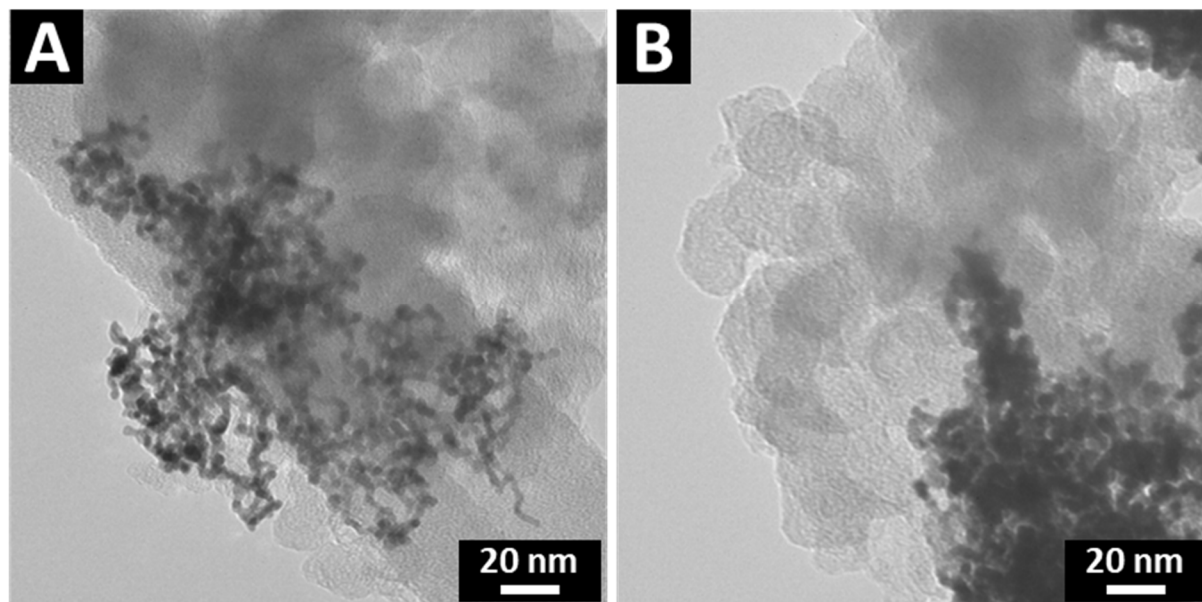


**SI Figure 11.** TEM images of (A) Pt<sub>1</sub>Ru<sub>9</sub>/C OAm before MOR, (B) Pt<sub>1</sub>Ru<sub>9</sub>/C OAm after MOR, (C) Pt<sub>1</sub>Ru<sub>1</sub>/C OAm before MOR, and (D) Pt<sub>1</sub>Ru<sub>1</sub>/C OAm after MOR.





**SI Figure 12.** TEM images of (A) Pt<sub>3</sub>Ru<sub>1</sub>/C CTAB before MOR, (B) Pt<sub>3</sub>Ru<sub>1</sub>/C CTAB after MOR, (C) Pt<sub>1</sub>Ru<sub>1</sub>/C CTAB before MOR, and (D) Pt<sub>1</sub>Ru<sub>1</sub>/C CTAB after MOR.



**SI Figure 13.** TEM images of Pt/C (A) before MOR and (B) after MOR.

Sample	SA (mA/cm <sup>2</sup> )	Ref.
Ru <sub>56</sub> Pt <sub>44</sub> /C nanowires	<b>0.30 @ 0.48 V vs SCE</b>	13
Pt <sub>3</sub> Ru <sub>1</sub> /C nanowires	<b>0.75 @ 0.65 V vs RHE</b>	14
PtRu nanodendrites	<b>2.66 @ 0.91 V vs RHE</b>	15
PtRu nanowires	<b>3.93 @ 0.90 V vs RHE</b>	16
PtRu nanocrystals	<b>1.16 @ 0.70 V vs SCE</b>	17
Pt/Ru/C nanocomposites	<b>1.20 @ 0.60 V vs RHE</b>	18
PtRu Icosahedra	<b>0.76 @ 0.90 V VS RHE</b>	19
Pt <sub>1</sub> Ru <sub>1</sub> @NC/C	<b>1.36 @ 0.70 V vs RHE</b>	20
Pt <sub>3</sub> Ru <sub>1</sub> /C	<b>1.22 @ 0.7 V vs RHE</b>	This Work

**SI Table 5.** Comparison with previously published results for MOR on various PtRu systems.

## References

1. A.-K. Shukla, M.-K. Ravikumar and K.-S. Gandhi, *J. Solid State Electrochem.*, 1998, **2**, 117-122.
2. A. S. Aricò, S. Srinivasan and V. Antonucci, *Fuel Cells*, 2001, **1**, 133-161.
3. C. Y. Chen, D. H. Liu, C. L. Huang and C. L. Chang, *J. Power Sources*, 2007, **167**, 442-449.
4. K. I. Ozoemena, *RSC Advances*, 2016, **6**, 89523-89550.
5. F. Vigier, S. Rousseau, C. Coutanceau, J.-M. Leger and C. Lamy, *Topics in Catalysis*, 2006, **40**, 111-121.
6. S. H. Joo, S. J. Choi, I. Oh, J. Kwak, Z. Liu, O. Terasaki and R. Ryoo, *Nature*, 2001, **412**, 169-172.
7. E. Antolini, J. R. C. Salgado and E. R. Gonzalez, *Appl. Catal., B*, 2006, **63**, 137-149.
8. Y. Shao, G. Yin and Y. Gao, *J. Power Sources*, 2007, **171**, 558-566.
9. H. Liu, C. Song, L. Zhang, J. Zhang, H. Wang and D. P. Wilkinson, *J. Power Sources*, 2006, **155**, 95-110.
10. J. Zhang, M. B. Vukmirovic, Y. Xu, M. Mavrikakis and R. R. Adzic, *Angew. Chem., Int. Ed.*, 2005, **44**, 2132-2135.
11. J. Zhang, K. Sasaki, E. Sutter and R. R. Adzic, *Science*, 2007, **315**, 220-222.
12. S. C. McGuire, A. M. Ebrahim, N. Hurley, L. Zhang, A. I. Frenkel and S. S. Wong, *Chem Sci*, 2021, **12**, 7158-7173.
13. W. Zhao, D. Huang, Q. Yuan and X. Wang, *Nano Research*, 2016, **9**, 3066-3074.
14. M. E. Scofield, C. Koenigsmann, L. Wang, H. Liu and S. S. Wong, *Energy & Environmental Science*, 2015, **8**, 350-363.
15. S. Zhang, H. Rong, T. Yang, B. Bai and J. Zhang, *Chemistry*, 2020, **26**, 4025-4031.
16. M. Li, Y. Wang, J. Cai, Y. Li, Y. Liu, Y. Dong, S. Li, X. Yuan, X. Zhang and X. Dai, *Dalton Trans*, 2020, **49**, 13999-14008.
17. L. Huang, X. Zhang, Q. Wang, Y. Han, Y. Fang and S. Dong, *J Am Chem Soc*, 2018, **140**, 1142-1147.
18. J. Gu, W.-C. Liu, Z.-Q. Zhao, G.-X. Lan, W. Zhu and Y.-W. Zhang, *Inorg. Chem. Front.*, 2014, **1**, 109-117.
19. Z. Lin, W. Chen, Y. Jiang, T. Bian, H. Zhang, J. Wu, Y. Wang and D. Yang, *Nanoscale*, 2016, **8**, 12812-12818.
20. Q. Wang, S. Chen, J. Jiang, J. Liu, J. Deng, X. Ping and Z. Wei, *Chem Commun (Camb)*, 2020, **56**, 2419-2422.